View metadata, citation and similar papers at core.ac.uk
brought to you by CORE
provided by Tokushima University Institutional Repository

Title: Practical method for determination of air kerma by use of an ionization chamber toward construction of a secondary X-ray field to be used in clinical examination rooms

Authors:

Itsumi MAEHATA[1)], Hiroaki HAYASHI[2,#)], Natsumi KIMOTO[1)],

Kazuki TAKEGAMI[3)], Hiroki OKINO[3)], Yuki KANAZAWA[2)], Masahide TOMINAGA[2)]

1) School of Health Sciences, Tokushima University

3-18-15 Kuramoto-Cho, Tokushima, Tokushima 770-8503, Japan

2) Institute of Biomedical Sciences, Tokushima University Graduate School

3-18-15 Kuramoto-Cho, Tokushima, Tokushima 770-8503, Japan

3) Graduate School of Health Sciences, Tokushima University

3-18-15 Kuramoto-Cho, Tokushima, Tokushima 770-8503, Japan

Corresponding Author:

Hiroaki HAYASHI

Institute of Biomedical Sciences, Tokushima University Graduate School

3-18-5 Kuramoto-cho, Tokushima, Tokushima 770-8503, Japan

+81-88-633-9054

hayashi.hiroaki@tokushima-u.ac.jp

Keywords: ionization chamber, air kerma, contamination rate, scattered X-rays, diagnostic X-ray equipment, secondary X-ray field

Abstract

We propose a new practical method for the construction of an accurate secondary X-ray field by use of medical diagnostic X-ray equipment. For accurate measurement of the air kerma of an X-ray field, it is important to reduce and evaluate the contamination rate of scattered X-rays. In order to determine the rate quantitatively, we performed the following studies. First, we developed a shield box in which an ionization chamber could be set at an inner of the box to prevent detection of the X-rays scattered from the air. In addition, we made collimator plates which were placed near the X-ray source for estimation of the contamination rate by scattered X-rays from the movable diaphragm which is a component of the X-ray equipment. Then, we measured the exposure dose while changing the collimator plates, which had diameters of 25-90 mm$^{\phi}$. The ideal value of the exposure dose was derived mathematically by extrapolation to 0 mm$^{\phi}$. Tube voltages ranged from 40 kV to 130 kV. Under these irradiation conditions, we analyzed the contamination rate by the scattered X-rays. We found that the contamination rates were less than 1.7% and 2.3%, caused by air and the movable diaphragm, respectively. The extrapolated value of the exposure dose has been determined to have an uncertainty of 0.7%. The ionization chamber used in this study was calibrated with an accuracy of 5%. By using kind of this ionization chamber, we can construct a secondary X-ray field

with an uncertainty of 5%.

1. Introduction

Currently, X-ray examinations are widely used for diagnosis in the medical field, and the risk of cancer in Japan caused by the diagnostic X-rays is estimated to have the highest value in the world **[1]**. Radiologic technologists should make efforts to reduce patient doses in addition to improving image quality **[2]**. In the diagnostic X-ray region, reducing the entrance skin dose (ESD) **[3]** is important, in addition to optimizing the exposure dose. Generally speaking, the ESD is estimated in terms of the air kerma with a correction for the back-scatter factor (BSF). The original idea for this procedure was reported previously **[4,5]**, and recently Kato proposed a new method for calculating the BSF [**6**]. Because the BSF is determined accurately, technologists need to measure the air kerma with ionization chambers. Generally speaking, the ionization chambers should be calibrated well with a standard X-ray field in which monoenergetic sources can be provided within the special large room to reduce contamination by scattered X-rays. Some institutions can provide calibration factors with accuracies of several percent, but the calibrations are expensive and not convenient. If we can construct a secondary X-ray field by using medical diagnostic X-ray equipment, inexpensive and convenient calibrations will be available. As is generally known, the experimental environment by means of medically-used X-ray equipment has many limitations; continuous X-rays with

63 contamination by scattered X-rays are generated. If these disadvantages caused by the
64 use of the diagnostic X-ray equipment are evaluated quantitatively, the secondary X-ray
65 field will become valuable under the limitation.

66 The diagnostic X-ray equipment used in clinics consists of an X-ray tube and a
67 movable diaphragm. It is well known that the movable diaphragm generates scattered
68 X-rays **[7-9]**. Therefore, the contributions of the scattered X-rays to the direct X-rays
69 should be estimated. Recently, Takegami *et al.* developed and suggested a new
70 collimator that has multiple-stage shields to reduce scattered X-rays coming from the
71 movable diaphragm **[8]**, but the irradiation area formed by the equipment is limited to a
72 relatively small area **[9]**. For calibration of an ionization chamber without the
73 contamination of scattered X-rays, a relatively large irradiation area will be needed. We
74 propose here a new method for a practical calibration method used in the secondary-X-
75 ray field.

76 **Figure 1 (a)** illustrates the ideal situation in which we measure only direct X-
77 rays with an ionization chamber. In reality, scattered X-rays are additionally
78 superimposed on the direct X-rays, as shown in **Fig.1 (b)**; (A) and (B) indicate scattered
79 X-rays generated by air and by the movable diaphragm, respectively. **Figure 1 (c)**
80 shows a schematic drawing of the method we propose in this study. The ionization

chamber is located in a shield box, which was newly developed for the reduction of scattered X-rays generated by air (indicated by (A) in **Fig. 1 (c)**). Also, a collimator plate is placed in front of the movable diaphragm. In order to estimate the contamination rate due to scattered X-rays (indicated by (B) in **Fig. 1 (c)**), we applied an extrapolation method **[10]** in which experimental values associated with different collimator plates are measured. In general, the exposure doses are analyzed based on the X-ray quality, which is described by the half-value layers (HVLs) **[11]** of aluminum. Appropriate research on the above-mentioned extrapolation method for deriving accurate half-value layers has been performed **[12,13]**. We applied the extrapolation method to correct the exposure dose measured with an ionization chamber.

In this paper, we propose a new method for constructing the secondary X-ray field by using medical diagnostic X-ray equipment, and we developed a shield box for the reduction of contamination from scattered X-rays. The rates of contamination by scattered X-rays were determined, and we also evaluated the precision and accuracy of the air kerma that was determined.

2. Materials and methods

2-1. Exposure dose measurements with ionization chambers

2-1-1. Development of apparatus

Figure 2 shows a schematic drawing of the shield box which was newly developed. We used commercially available materials to develop the apparatus. The outer size of this shield box was 284 mm high, 334 mm wide, and 300 mm long. The sides of the box were composed of 2 mm lead supported by 2 mm aluminum. We did not add a shield at the back surface to prevent unnecessary scattered X-rays, which are generated by the shield. The front surface was made of 2 mm aluminum and 2 mm lead, and in addition to this, 2 mm of copper was used for reducing the characteristic X-rays from lead **[14]**. The incident X-rays were limited by a shield-box-collimator placed at the center of the front surface of the shield box. The size of this shield-box-collimator, consisted of 2 mm aluminum and 2 mm lead, was 210 mm × 165 mm, and had a diameter of 100 mm$^{\phi}$. According to a well-known database **[15]**, the mean range of secondary electrons produced with X-rays having a tube voltage of 130 kV (effective energy of 42 keV) was estimated to be 42 mm; therefore, the irradiation area formed by the shield-box-collimator of 100 mm$^{\phi}$ was sufficient for achieving secondary-electron equilibration. The ionization chamber was held together by a clamp which was fixed to the upper side of the shield box. At the rear of the shield box, a phosphor plate can be set to confirm both the irradiation area and the position of the ionization chamber by use

of X-rays.

The collimator plates placed in front of the movable diaphragm (see **Fig. 1 (c)**) were composed of lead and aluminum, each 210 mm high, 165 mm wide, and 2 mm thick. A hole was bored through the center of the plate. The diameters of the holes were 25 mm$^{\phi}$, 30 mm$^{\phi}$, 40 mm$^{\phi}$, 50 mm$^{\phi}$, 60 mm$^{\phi}$, 70 mm$^{\phi}$, 80 mm$^{\phi}$, and 90 mm$^{\phi}$.

2-1-2. Experimental procedures

In order to measure exposure doses, we used diagnostic X-ray equipment (MRAD-A 50S/70, Toshiba Medical Systems Corporation, Nasu, Japan), collimator plates, a shield box, ionization chambers having a 3 cc detection volume (DC300, PTW, Freiburg, Germany) and a 0.6 cc detection volume (30013 type, PTW, Freiburg, Germany), a dosimeter (EMF521, EMF Japan Ltd., Osaka, Japan) for ionization chambers. With help of the schematic drawing of **Fig. 1** (c), we explain the experiment. **Figure 3** shows photographs of the experimental set up. Our experiments were performed under the following four conditions: in setup A, the ionization chamber was located in the shield box, and in setup B, the ionization chamber was placed in a free-air condition (without shield box). For these conditions, ionization chambers having different detection volumes were used; one had a detection volume of 0.6 cc and the other,

3 cc. By use of a commercially available standard X-ray field (Japan Quality Assurance (JQA) organization, Japan), the calibration factors of the ionization chambers were determined to be 13.91×10^5 (C/kg)/C for the 0.6 cc chamber and $2.83\text{-}2.99\times10^5$ (C/kg)/C for the 3 cc chamber, with an uncertainty of 5%. The temperature and air pressure were recorded, and the values measured with the ionization chambers were corrected so as to agree with the standard temperature and pressure **[16]**. The collimator plates for applying the extrapolation method were placed near the movable diaphragm (35 cm from the X-ray source), as shown in the graph on the right in **Fig. 3**. An acrylic guide for the collimator plates was set on a tripod for easy adjustment. The distances between the X-ray source and the collimator-plate and ionization chamber were 35 cm and 250 cm, respectively. Movable diaphragms was full open; the size of the irradiation area at the end of an emission port is formed to be 13 cm × 13 cm at the distance of 27 cm from the X-ray source. Irradiation conditions were a current of 200 mA, an irradiation time of 0.5 s, and tube voltages of 40 kV, 70 kV, 100 kV, and 130 kV. For each condition, five measurements were performed for estimates of the statistical uncertainty **[14]**.

Before measurements with the ionization chambers, we set a phosphor plate (RP-4S, Konica Minolta Health Care Co., Ltd., Tokyo, Japan) at the rear of the shield box to check the X-ray irradiation area and the position of the ionization chambers. In order to

check the exposure doses preliminary, the pixel value in the obtained image was analyzed using a software ImageJ [**17**]. Then, based on the following mathematical formula between digital value (DV) and dose (D), we estimated the doses from the pixel values **[18,19]**;

$$D \propto \mathrm{Exp}(0.00218 \times DV). \quad (1)$$

We used derived values to check the consistency of the measured values between the ionization chambers and the phosphor plates.

2-1-3. Analysis

We describe the extrapolation method for estimating the contamination rate of scattered X-rays measured with ionization chambers. According to that method **[10]**, the amount of scattered X-rays is considered to be proportional to the diameter of the collimator plates which are set in front of the X-ray equipment. Here, the adopted value corresponding to the ideal situation in **Fig. 1 (a)** can be obtained when we plot the measured values as a function of the diameter of the collimator plates, 25 mm$^{\phi}$ to 90 mm$^{\phi}$, and the extrapolated values to 0 mm$^{\phi}$. Note that the X axis is diameters of the collimator plates, and not the diameters of the irradiation field. In our experiments, the detection part of the ionization chamber was covered fully in the irradiation field even when the

collimator plate of 25 mm$^{\phi}$ was used. For the extrapolation, a linear function was used, and the weighted least-squares method was applied. Simultaneously, we estimated the uncertainty of the extrapolated value by consideration of the statistical uncertainty of the measured values [C] of the ionization chambers. Then, the air kerma [J/kg] was obtained by multiplying both the calibration factor [(C/kg)/C] and the "W-value divided by the elemental charge e" of 33.97 [J/C] **[15]** to the measured value [C].

2-2. Exposure dose measurements using a CdTe detector

2-2-1. Experimental procedure

In order to check the effectiveness of the shield box based on a different procedure, we also measured the X-ray spectra by using a CdTe detector (EMF123, EMF Japan Ltd., Osaka, Japan) **[20,21]**. Setups C and D in **Fig. 3** show experimental setups with use of the CdTe detector with and without the shield box, respectively; the CdTe detector was set in the place by use of a camera platform. The irradiation conditions were as follows: 70 kV, 200 mA, and 0.5 s. We applied the Compton scatter spectroscopy method (scattering angle of 90 degrees) proposed by Maeda *et al*. **[22]**. A carbon scatterer was used in place of the ionization chamber (see **Fig. 3**). In our experimental conditions, the counting rate (counts per seconds: CPS) of the CdTe detector

189 was kept below 1 kCPS to reduce the pulse pileup effect **[23,24]**.

190

191 2-2-2. Analysis

192 In order to analyze the exposure dose by use of the measured X-ray spectra of
193 the CdTe detector, we applied the following analysis. First, by use of the Klein-Nishina
194 formula and the response function of the CdTe detector, originally measured spectra were
195 unfolded **[22]**. Then, we transformed the X-ray spectra Φ(E) to air kerma by using the
196 following equation:

197 $$\text{Air kerma} = \int \Phi(E) \times E \times \left(\frac{\mu_{tr}(E)}{\rho}\right) dE, \quad (2)$$

198 where E and $\mu_{tr}(E)/\rho$ are the energy **[25]** and the mass energy transfer coefficient,
199 respectively.

200

201 3. Results

202 3-1. Exposure dose measurements by use of ionization chambers

203 **Figure 4** shows X-ray images of the phosphor plate which we used to check the
204 irradiation areas of the 3 cc chamber in setup A. **Figures 4 (a)** and **(b)** indicate the
205 results based on the collimator plates of 25 mm^{ϕ} (smallest) and 90 mm^{ϕ} (largest),
206 respectively. It is clearly seen that the detection area of the ionization chamber is

included sufficiently in the irradiation area. From a geometrically based consideration, irradiation areas of 178 mm$^{\phi}$ and 642 mm$^{\phi}$ can be formed by use of the collimator-plates of 25 mm$^{\phi}$ and 90 mm$^{\phi}$, respectively, in setup B (without a shield box) at the position where the chamber was set. On the other hand, in setup A (with a shield box), both irradiation areas were limited to be 114 mm$^{\phi}$, as shown in **Fig. 4**. This was caused by the shield-box-collimator of 100 mm$^{\phi}$ placed in front of the shield box. In the irradiation parts in the figure, DVs measured with the phosphor plate not including the ionization chamber are also shown; namely, DV of 3537.5±0.9 for the 25 mm$^{\phi}$ collimator plate, and that of 3542.2±0.9 for the 90 mm$^{\phi}$ collimator plate. From equation (1), the relative doses corresponding to the collimator plates of 25 mm$^{\phi}$ and 90 mm$^{\phi}$ were estimated to be 1.000±0.002 and 1.010±0.002, respectively. The difference in values was consistent with the result, which is presented in the next paragraph (**Fig. 5 (b)**).

Figures 5 (a)-(d) shows a comparison of exposure doses measured with ionization chambers between setup A (with a shield box, solid circles) and setup B (without a shield box, open circles) in **Fig. 3** for four tube voltages. The results of 3 cc chamber are presented. The X-axis shows the diameter of the collimator plate. A linear function was applied for fitting to the experimental data, and an extrapolated data corresponding to 0 mm$^{\phi}$ was obtained. Then the exposure doses were normalized by the

225 extrapolated value, and the normalized values are plotted on the Y-axis. It is clearly seen
226 that the data measured without the shield box are systematically larger than those with
227 the shield box. The differences in data with or without the shield box at 40 kV, 70 kV,
228 100 kV, and 130 kV were 0.9%, 1.3%, 1.1%, and 1.0%, respectively. The error bars in
229 the figure are standard deviations of the measured values for five measurements, and in
230 the extrapolated value, the contribution of these uncertainties is considered. As a result,
231 the statistical uncertainties of the extrapolated data for 40 kV, 70 kV, 100 kV, and 130 kV
232 were approximately 0.5%, 0.2%, 0.1%, and 0.3%, respectively.

233 **Figure 6 (a)** shows a comparison of the results for the two ionization chambers.
234 The solid and open circles indicate the results for the 3 cc and 0.6 cc chambers,
235 respectively. All of the air-kerma values measured with the 0.6 cc chamber are
236 consistent with those of the 3 cc chamber. This result indicates that our experiments did
237 not depend on the volume of the ionization chambers.

238

239 3-2. Exposure dose measurements with the CdTe detector

240 **Figure 6 (b)** shows X-ray spectra measured with a CdTe detector with or without
241 the shield box. The X axis shows the energy [keV], and the Y axis shows the counts.
242 Using equation (2), we derived corresponding dose with the spectra; the relative values

of derived air kerma of the conditions with (setup C in **Fig. 3**) and without the shield box (setup D in **Fig. 3**) were 1.000±0.002 and 1.018±0.002, respectively. As described above, the results measured with the ionization chamber shown in **Fig. 5 (b)** indicate a 1.6% difference between measured values with and without the shield box with use of the 90 mm$^{\phi}$ collimator plate; the result with the CdTe detector was consistent with that of the ionization chamber.

4. Discussion

In the present study, we proposed an accurate measurement method for air kerma by use of diagnostic X-ray equipment. In general, diagnostic X-ray equipment has a movable diaphragm, and this becomes a generator of scattered X-rays. To construct an accurate X-ray field, we proposed to use a shield box to reduce the scattered X-rays, and we estimated the contamination rate by the scattered X-rays.

It was considered that a free-air condition is suitable for calibration of ionization chambers. We consider that our method is applicable only to the diagnostic X-ray region, and that it is useful for reducing scattered X-rays from the movable diaphragm of clinical X-ray equipment. As described above, the experiments were validated because the contamination rate by the scattered X-rays measured with one ionization chamber was

consistent with that measured with another ionization chamber, the phosphor plate, and the CdTe detector. This finding strongly support the verification of our method. Next, we describe the evaluation of the accuracy of our method.

As shown in **Fig. 5**, the extrapolation method works well because experimental data deviated evenly from a linear fitted line. The effect of the shield box was clearly presented by the data; the open circles (setup B, without a shield box) were systematically larger than the closed circles (setup A, with a shield box). Here, we estimate the differences between these data corresponding to the X (diameter of shield-box-collimator) = 100 mm$^{\phi}$. As represented in **Fig. 5**, they were 1.5-1.7% for tube voltages of 40-130 kV. The differences are considered to be due to contamination by scattered X-rays from air, which is indicated by (A) in **Fig. 1 (b)**. Reducing these scattered X-rays is important for deriving an accurate exposure dose, because the extrapolated data (related to the 0 mm$^{\phi}$ of the collimator plate) became systematically 0.9-1.3% larger than the ideal values when extrapolation was applied to setup B (without a shield box). From these findings, we concluded that a more accurate value of exposure dose can be obtained with use of our shield box.

Here, we also discuss the contamination rate of scattered X-rays from a movable diaphragm, which is indicated by (B) in **Fig. 1 (b)**. In **Fig. 5**, the amount of these X-

279 rays was observed by the differences between the extrapolated value of the exposure dose
280 and other data in setup A (with a shield box). In the present case, scattered X-rays from
281 the movable diaphragm were estimated to be at most 1.8-2.3%. Although these
282 estimated values are not common, they become a good example to explain our method
283 when experiments are performed with diagnostic X-ray equipment installed in clinical
284 examination rooms.

285 **Figure 7** shows a relationship of the extrapolated values of the exposure dose in
286 terms of the measured values [C] and air kerma [J/kg] at 70 kV. In the dimension of the
287 measured value [C], statistical uncertainty is considered only to these data. In the
288 present case, the statistical uncertainty of the extrapolated value was 0.7%, as represented
289 by the right-hand graph in **Fig. 7**. On the other hand, as shown in the left graph in **Fig.**
290 **7**, the uncertainty of the air kerma (extrapolated value) was determined by consideration
291 of both the statistical uncertainty (0.7%) and the uncertainty of the calibration factor (5%).
292 Therefore, the final uncertainty of the measured value becomes approximately 5%.

293 When we want to calibrate another ionization chamber by using our secondary
294 X-ray field, the ionization chamber can be calibrated with 5% uncertainty. At this time,
295 the calibration factor has a larger uncertainty compared with the contribution of scattered
296 X-rays. However, if we can use an accurately calibrated ionization chamber, our

297 method of using a shield box may be more valuable. Our secondary X-ray field will
298 also play an important role in the calibration not only of ionization chambers, but also of
299 other radiation detectors such as solid detectors. We plan to calibrate an optically
300 stimulated luminescence (OSL) dosimeter by using our secondary X-ray field. The
301 detection efficiency of the OSL dosimeter is completely different from that of the
302 ionization chambers; for example, the relative efficiency of 20 keV X-rays is 20% larger
303 than that of 60 keV [**26**]. In other words, when an experimenter calibrates the OSL
304 dosimeter, the contribution of low energy X-rays (scattered X-rays) should be considered.
305 With the proposed calibration method, it is hoped that the contribution of the scattered X-
306 rays is properly estimated; firstly, the ionization chamber for standard is measured and
307 analyzed by the proposed method (as represented in **Fig. 5**), secondary, a radiation
308 detector which experimenter wants to calibrate is measured with the same condition and
309 also analyzed with the proposed method, and then, the extrapolated values are compared.
310 In this procedure, the effect of the low energy X-ray contamination on each detector was
311 properly corrected.
312
313 5. Conclusion
314 In conclusion, we proposed a practical calibration method for which we used an

original shield box and collimator plates to prevent scattered X-rays, and we evaluated the contamination rates by them for construction of a secondary X-ray field by means of general diagnostic X-ray equipment. Our equipment is portable; we considered that our equipment was useful for calibration of ionization chambers with X-ray equipment used in clinical examination rooms. We applied the method to a general experimental room in Japan, and we found that the contamination rates of scattered X-rays from the air and the movable diaphragm were less than 1.7% and 2.3%, respectively. The precision and accuracy of the extrapolation method were approximately 0.7% in the measured value [C], and 5% in the air kerma [J/kg]. We found that our method was more accurate than the uncertainty of the calibration factor used. Our method will become valuable when a more accurately calibrated ionization chamber is available.

Conflict of interest

We have no conflict of interest.

6. References

[1] Amy Berrington de Gonzalez, Sarah Darby. Risk of cancer from diagnostic X-ray: estimates for the UK and 14 other countries. The Lancet. 2004;363:345-351.

[2] Uffmann M, Prokop CS. Digital radiography: The balance between image quality and required radiation dose. European Journal of Radiology. 2009;72:202-208.

[3] Takegami K, Hayashi H, Okino H, Kimoto N, Maehata I, Kanazawa Y, Okazaki T, Kobayashi I. Practical calibration curve of small-type optically stimulated luminescence (OSL) dosimeter for evaluation of entrance skin dose in the diagnostic X-ray region. Radiological Physics and Technology. 2015;8:286-294.

[4] Grosswendt B. Backscatter factors for x-rays generated at voltages between 10 and 100 keV. Physics in Medical and Biology. 1954;29(5):579-591.

[5] Klevenhagen SC. Experimentally determined backscatter factors for x-rays generated at voltages between 16 and 140 kV. Physics in Medical and Biology. 1989;34(12):1871-1882.

[6] Kato H, Method of calculating the Backscatter Factor for Diagnostic X-rays Using the Differential Backscatter Factor. Japanese Journal of Radiological Technology. 2001:57(12):1503-1510.

[7] Hayashi H, Taniuchi S, Kamiya N, et al. Development of a Pin-hole Camera Using a

348 Phosphor Plate, and Visualization of the Scattered X-ray Distribution and Optical
349 Image. Japanese Journal of Radiological Technology. 2012;68(3):307-311.
350 [8] Takegami K, Hayashi H, Konishi Y, et al. Development of multistage collimator for
351 narrow beam production using filter guides of diagnostic X-ray equipment and
352 improvement of apparatuses for practical training. Medical Imaging and Information
353 Sciences. 2013;30(4):101-107.
354 [9] Hayashi H, Takegami K, Okino H, et al. Procedure to measure angular dependences
355 of personal dosimeters using diagnostic X-ray equipment. Medical Imaging and
356 Information Sciences. 2015;32(1):8-14.
357 [10] Hayashi H, Takegami K, Konishi Y et al. Indirect Method of Measuring the Scatter
358 X-ray Fraction Using Collimators in the Diagnostic Domain. Japanese Journal of
359 Radiological Technology. 2014;70(3):213-222.
360 [11] Ariga E, Ito S, Deji S et al. Determination of half value layers of X-ray equipment
361 using computed radiography imaging plates. Physica Medica 2012;28:71-75.
362 [12] Trout ED, Kelley JP, and Lucas AC. Determination of Half-Value Layer. Radiology.
363 1959;73:107-108.
364 [13] Trout ED, Kelley JP, and Lucas AC. Determination of Half-Value Layer. The
365 American Journal of Roentgenology, Radium Therapy, and Nuclear Medicine.

366 1960;84(4):729-740.

367 [14] Knoll GF. Radiation Detection and Measurement third edition. John Wiley & Sons,

368 Inc. New York. 1999;321. ISBN 0-471-07338-5.

369 [15] Lucien P. Energy loss, range, and bremsstrahlung yield for 10-keV to 100-MeV

370 electrons in various elements and chemical compounds. Atomic Data and Nuclear

371 Data Tables. 1972;4:1-127.

372 [16] Khan FM. The Physics of Radiation Therapy fourth edition. Lippincott Williams &

373 Wilkins. 2010.

374 [17] Rasband WS, ImageJ, U. S. National Institutes of Health, Bethesda, Maryland, USA,

375 http://imagej.nih.gov/ij/, 1997-2015.

376 [18] Kimoto N, Hayashi H, Maehata I, et al. Development of All-in-one Multi-slit

377 Equipment for Measurements of the Input-output Characteristic of a Phosphor Plate,

378 Japanese Journal of Radiological Technology, 2013;69(10):1165-1171.

379 [19] Maehata I, Hayashi H, Takegami K, et al. Fabrication of Improved Multi-slit

380 Equipment to Obtain the Input-output Characteristics of Computed Radiography

381 Systems: Correction of the Heel Effect, and Application to High Tube-voltage

382 Experiments, Japanese Journal of Radiological Technology, 2014;70(9):867-876.

383 [20] Okino H, Hayashi H, Nakagawa K *et al*. Measurement of response function of CdTe

detector using diagnostic X-ray equipment and evaluation of Monte-Carlo simulation code, Japanese Journal of Radiation Radiological Technology, 2014;70(12):381-1391.

[21] Fukuda I, Hayashi H, Takegami K *et al*. Development of an experimental apparatus for energy calibration of a CdTe detector by means of diagnostic X-ray equipment, Japanese Journal of Radiation Radiological Technology, 2013;69 (9):952-959.

[22] Maeda K, Matsumoto M and Taniguchi A. Compton-scattering measurement of diagnostic x-ray spectrum using high-resolution Schottky CdTe detector. Med. Phys. 2005;32:1542-1547.

[23] Then SS, Geurink FDP, Bode P, et al. A pulse generator simulating Ge-detector signals for dead-time and pile-up correction in gamma-ray spectrometry in INAA without distortion of the detector spectrum. J. Radioanal. Nucl. Chem. 1997;215(2):249-252.

[24] Cano-Ott D, Tain JL, Gadea A. Pulse pileup correction of large NaI(Tl) total absorption spectra using the true pulse shape. Nucl. Instrum. Methods. 1999;430:488-497.

[25] Hubbell JH. Photon mass attenuation and energy-absorption coefficients, The International Journal of Applied Radiation and Isotopes, 1982;33(11):1269-1290.

[26] Takegami K, Hayashi H, Okino H, et al. Energy dependence measurement of small-

type optically stimulated luminescence (OSL) dosimeter by means of characteristic X-rays induced with general diagnostic X-ray equipment, Radiological Physics and Technology, in press (DOI: 10.1007/s12194-015-0339-9).

406 Figure captions:

407 Fig.1 Comparison between ideal, real conditions in measurments with ionization
408 chamber, and our proposed method. **(a)** Ideal condition of chamber; it measures only
409 direct X-rays. **(b)** Actual condition; it also measures scattered X-rays. **(c)** Our
410 proposed method for measuring only direct X-rays with an ionization chamber. There
411 are a newly developed box and collimator plates to shield from scattered X-rays. These
412 collimator plates have different diameters. (A) and (B) show scattered X-rays caused
413 by the air and the movable diaphragm, respectively.

414

415 Fig.2 Schematic drawings of our newly developed shield box which is 284 mm high,
416 334 mm wide, and 300 mm thick. The front surface is made of 2 mm lead, 2 mm
417 aluminum, and, in addition, 2 mm copper to absorb the characteristic X-rays of lead.
418 The ionization chamber is held by a clamp which is fixed to the upper side of the shield
419 box. For checking the irradiation area and a position of the ionization chamber, a
420 phosphor plate can be inserted at the back.

421

422 Fig.3 Experimental conditions for the X-ray equipment and the detectors. We
423 performed the experiment by using four conditions (setups A-D); different combinations

of two kinds of detectors, and with or without shield box.

Fig.4 X-ray images of a phosphor plate which was placed at the rear of the shield box. **(a)** and **(b)**: Results for 25 mm$^{\phi}$ and 90 mm$^{\phi}$ collimator plates. The detector was placed at the center of the irradiation field. The digital value (DV) of the image measured with the phosphor plate and the converted dose from the DV are given.

Fig.5 Experimental results measured with ionization chamber for 40 kV to 130 kV as a function of diameter of collimator plate. The Y-axis shows dose, which was normalized by the extrapolated value. The solid and open circles refer to the conditions of setup A (with a shield box) and setup B (without a shield box), respectively.

Fig.6 Verification of our method. **(a)** Comparison of the results for 70 kV between two different-size ionization chambers. The solid-circle data (3 cc chamber) and open circle data (0.6 cc chamber) are consistent with each other. **(b)** X-ray spectrum measured with the CdTe detector with and without the shield box. We plotted the original and unfolded spectra, in which the lines with solid and closed circles represent measured data with shield box and without it, respectively.

Fig.7 Uncertainty estimation of our method. The data in the right figure have statistical uncertainty. In this case, the extrapolated data have an uncertainty of 0.7%. The data in the left figure show the total uncertainty in which both the statistical uncertainty (0.7%) and that of the calibration factor (5%) are considered.

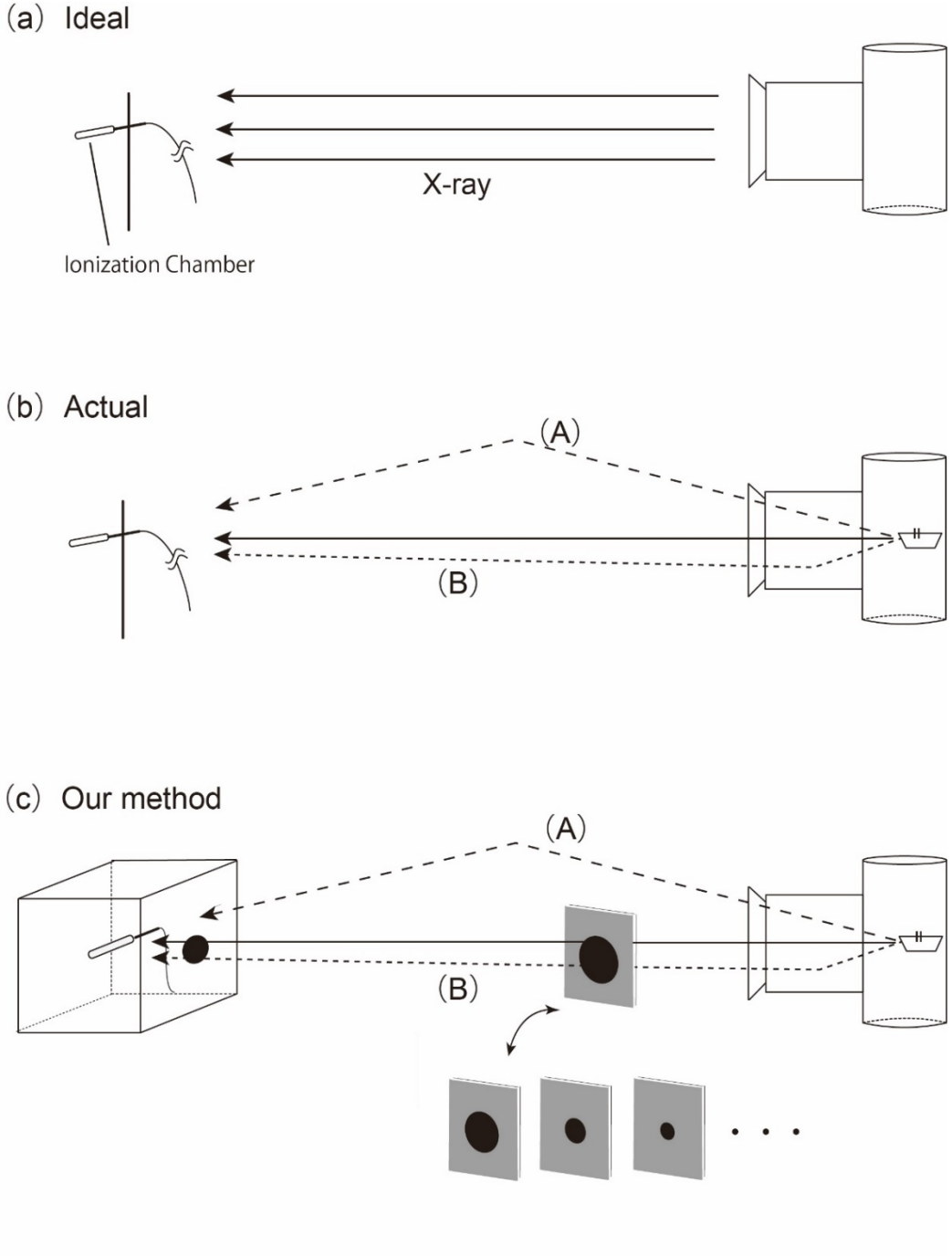

Fig.1

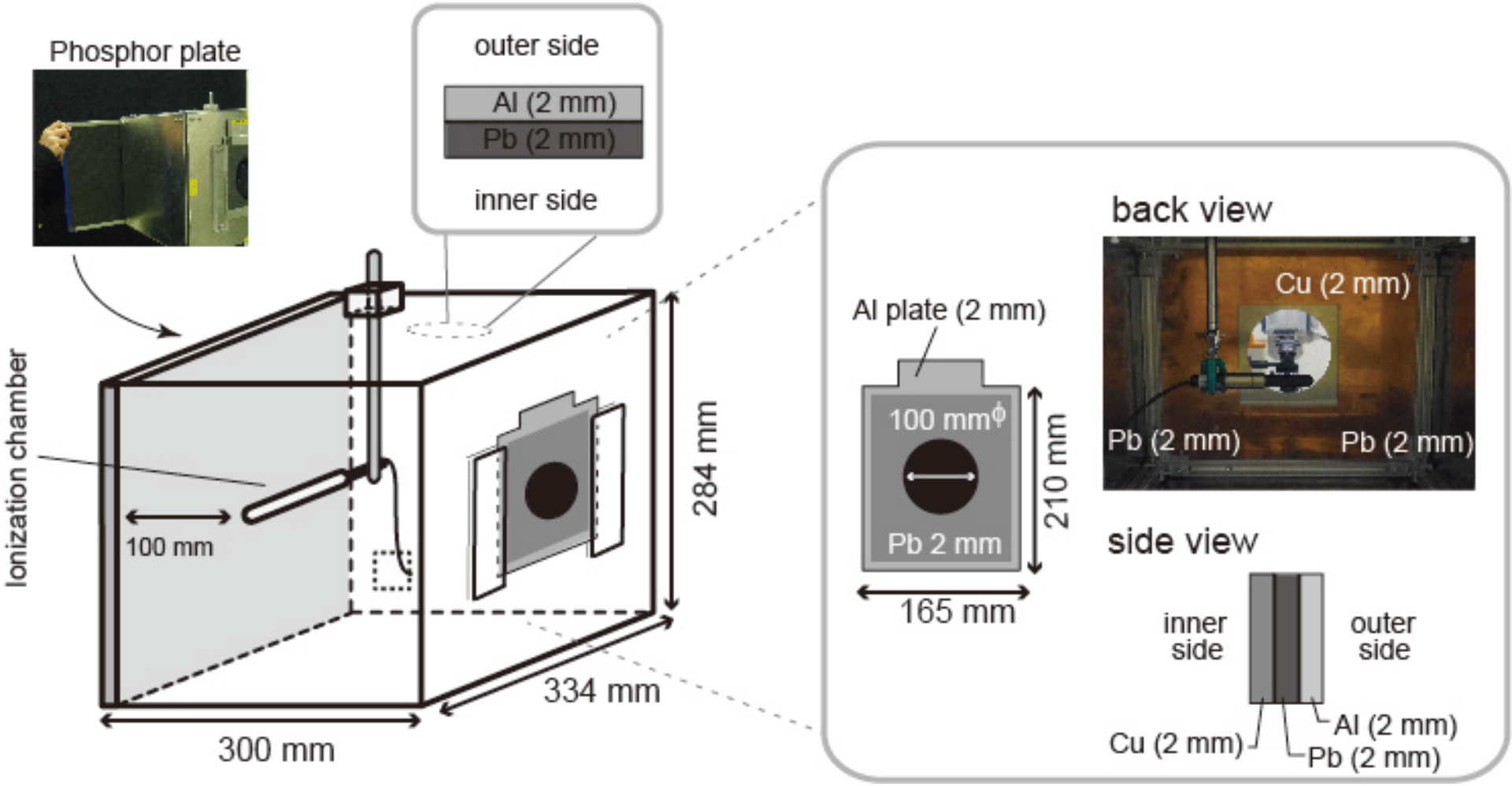
Phosphor plate
outer side
Al (2 mm)
Pb (2 mm)
inner side
Ionization chamber
100 mm
284 mm
334 mm
300 mm
Al plate (2 mm)
100 mmϕ
Pb 2 mm
210 mm
165 mm
back view
Cu (2 mm)
Pb (2 mm)
Pb (2 mm)
side view
inner side
outer side
Al (2 mm)
Cu (2 mm)
Pb (2 mm)

Fig.2

Detector

ionization chamber

setup A

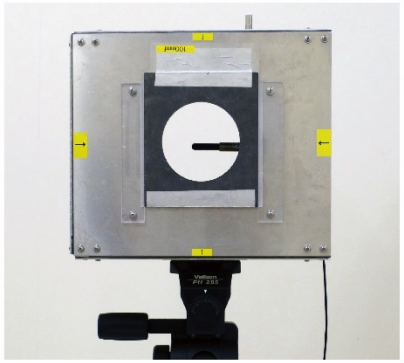

setup B

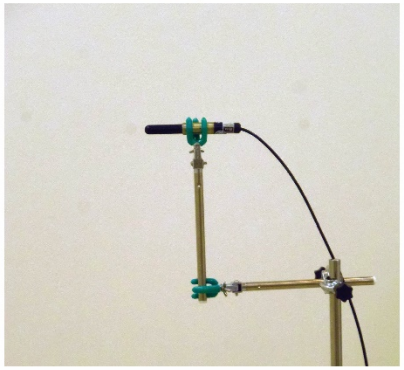

CdTe

setup C

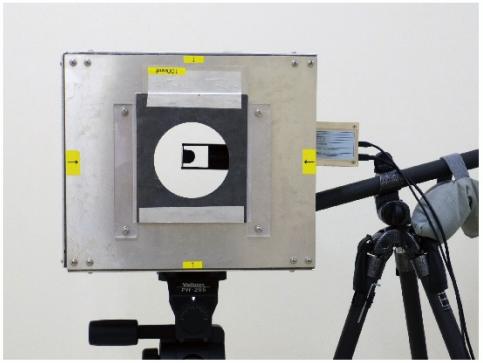

with shield box

setup D

without shield box

X-ray equipment

Fig.3

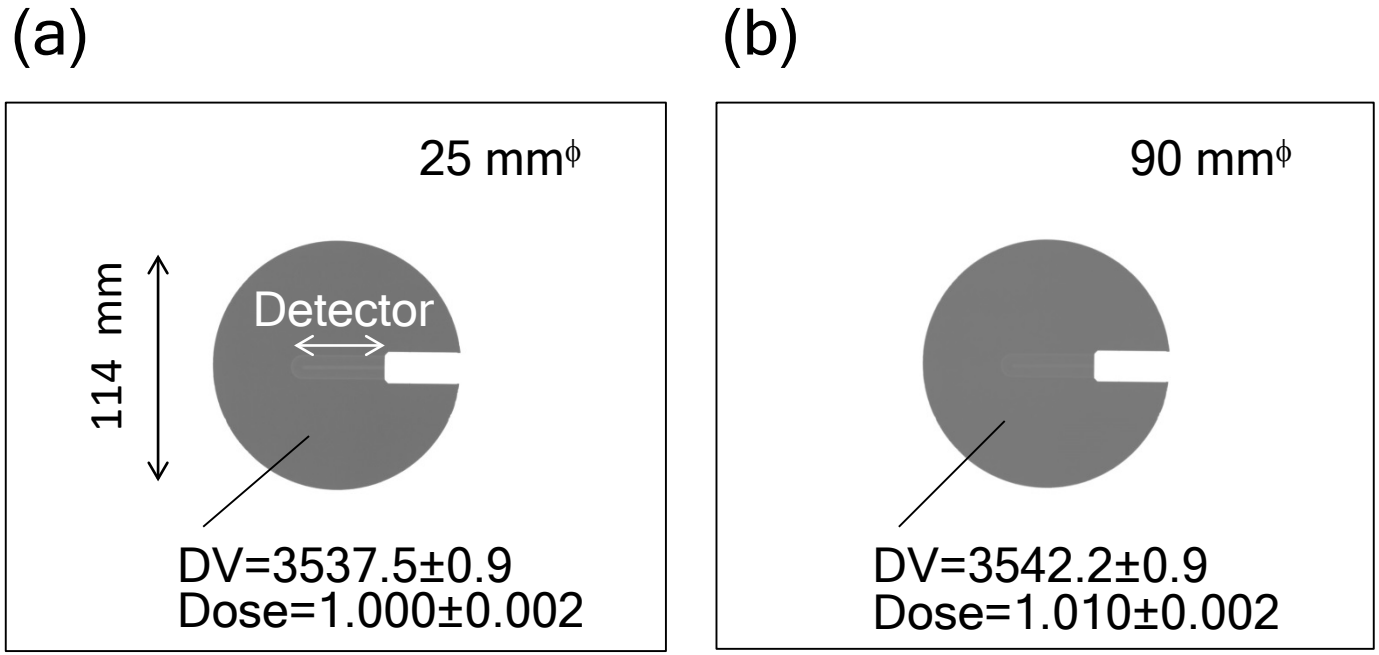
(a)
25 mmϕ
114 mm
Detector
DV=3537.5±0.9
Dose=1.000±0.002
(b)
90 mmϕ
DV=3542.2±0.9
Dose=1.010±0.002

Fig. 4

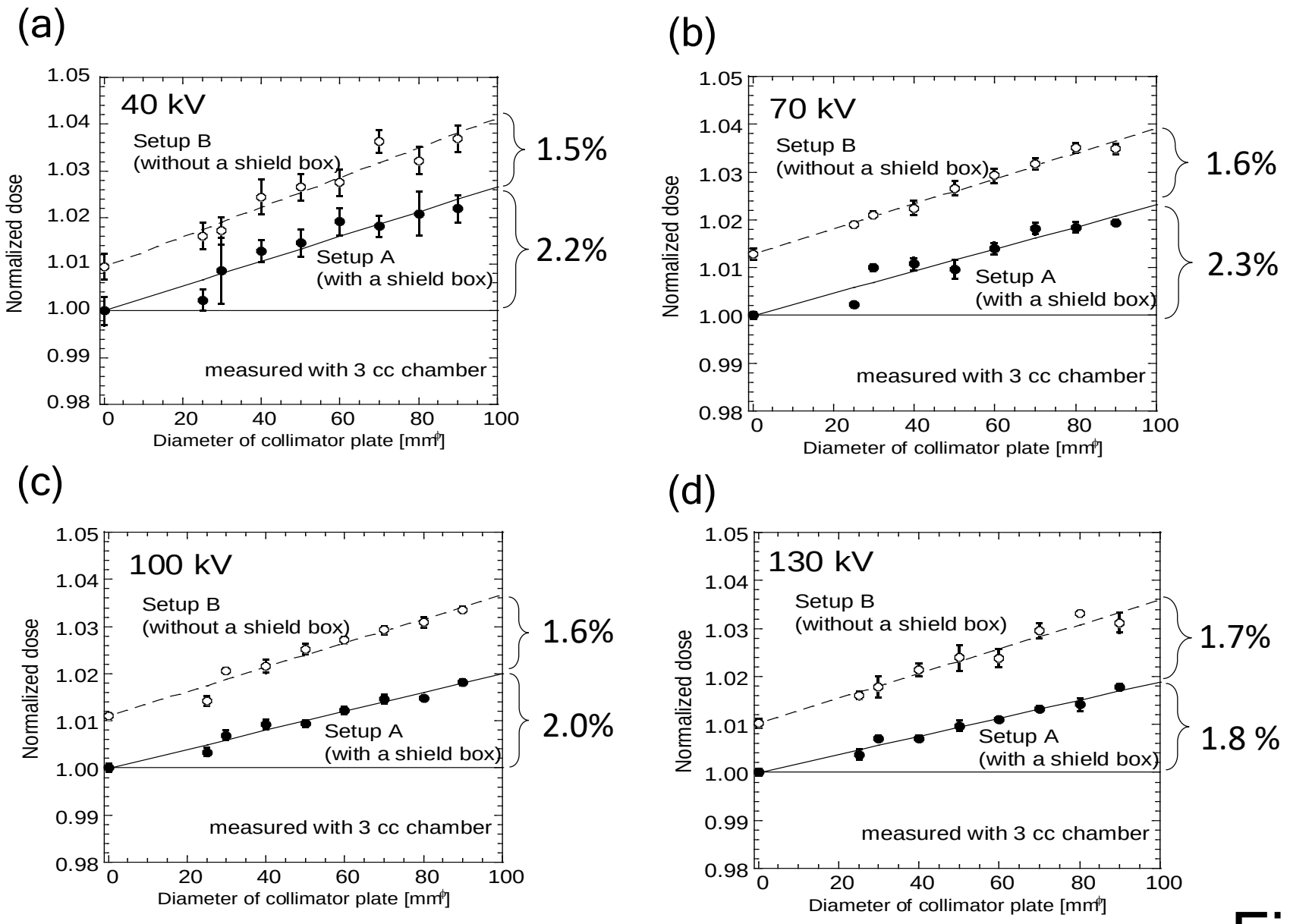
(a)
40 kV
Setup B
(without a shield box)
Setup A
(with a shield box)
1.5%
2.2%
measured with 3 cc chamber
Normalized dose
Diameter of collimator plate [mmϕ]
(b)
70 kV
Setup B
(without a shield box)
Setup A
(with a shield box)
1.6%
2.3%
measured with 3 cc chamber
Normalized dose
Diameter of collimator plate [mmϕ]
(c)
100 kV
Setup B
(without a shield box)
Setup A
(with a shield box)
1.6%
2.0%
measured with 3 cc chamber
Normalized dose
Diameter of collimator plate [mmϕ]
(d)
130 kV
Setup B
(without a shield box)
Setup A
(with a shield box)
1.7%
1.8 %
measured with 3 cc chamber
Normalized dose
Diameter of collimator plate [mmϕ]

Fig.5

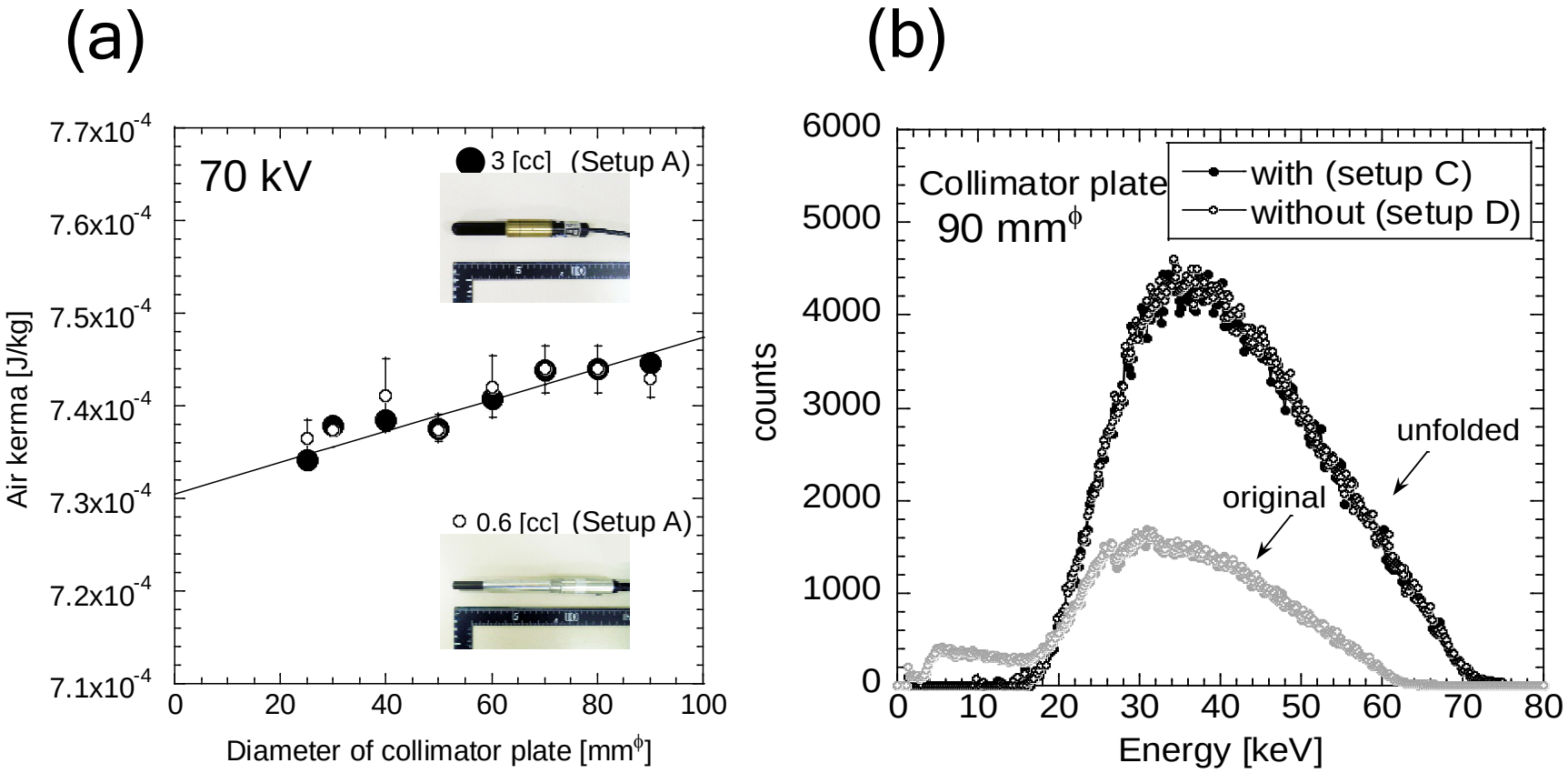
(a)
70 kV
3 [cc] (Setup A)
0.6 [cc] (Setup A)
Air kerma [J/kg]
7.7x10-4
7.6x10-4
7.5x10-4
7.4x10-4
7.3x10-4
7.2x10-4
7.1x10-4
0
20
40
60
80
100
Diameter of collimator plate [mmϕ]
(b)
Collimator plate
90 mmϕ
with (setup C)
without (setup D)
unfolded
original
counts
6000
5000
4000
3000
2000
1000
0
0
10
20
30
40
50
60
70
80
Energy [keV]

Fig. 6

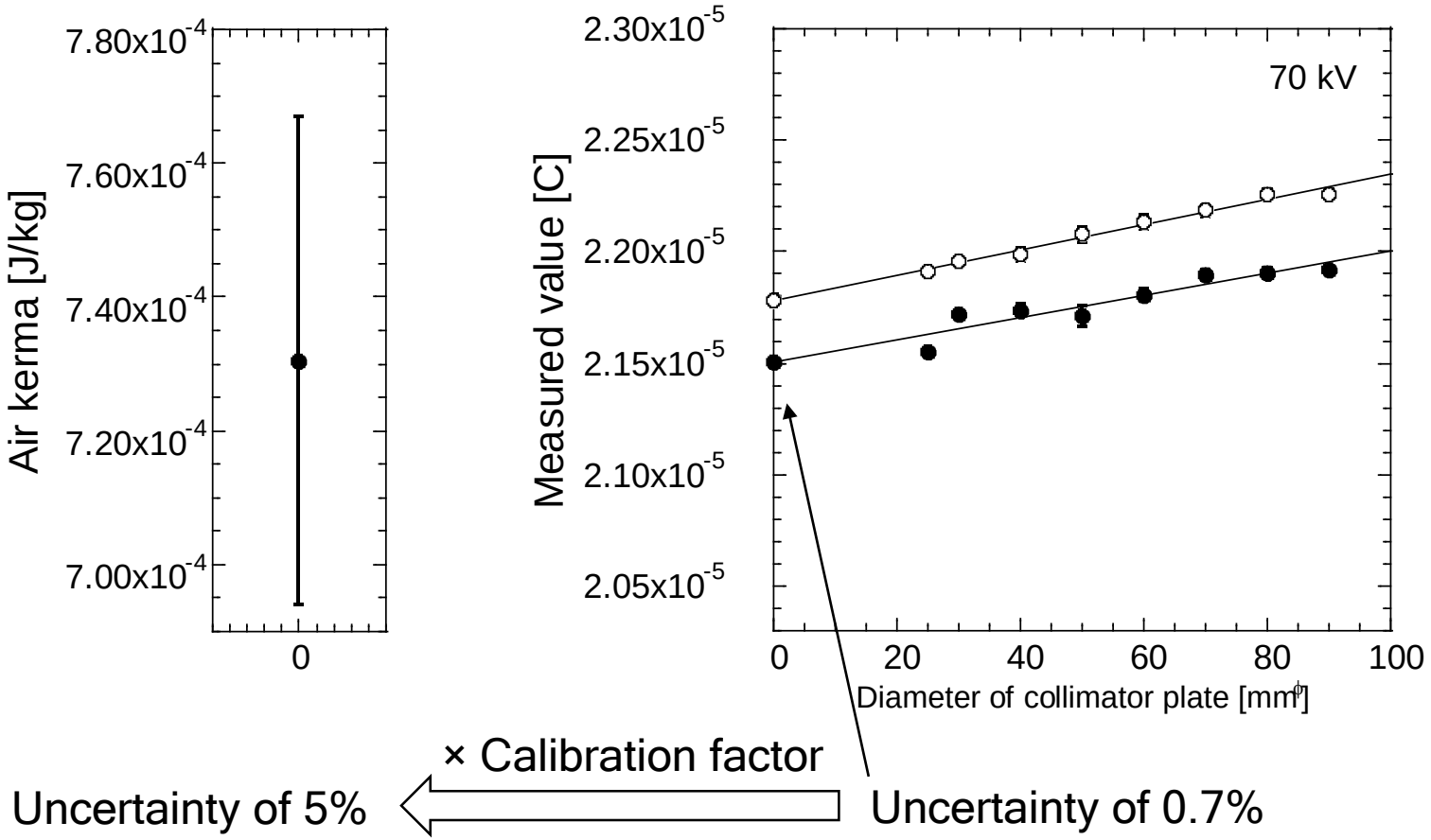
7.80x10-4
7.60x10-4
7.40x10-4
7.20x10-4
7.00x10-4
Air kerma [J/kg]
0
2.30x10-5
2.25x10-5
2.20x10-5
2.15x10-5
2.10x10-5
2.05x10-5
Measured value [C]
70 kV
0
20
40
60
80
100
Diameter of collimator plate [mmϕ]
× Calibration factor
Uncertainty of 5%
Uncertainty of 0.7%

Fig.7